Published in final edited form as:
Biomacromolecules. 2010 March 8; 11(3): . doi:10.1021/bm901298t.

Computational Insights into the Interactions between DNA and siRNA with "Rigid" and "Flexible" Triazine Dendrimers

Giovanni M. Pavan[*,†], **Meredith A. Mintzer**[‡], **Eric E. Simanek**[‡], **Olivia M. Merkel**[§], **Thomas Kissel**[§], and **Andrea Danani**[†]
University for Applied Sciences of Southern Switzerland (SUPSI) - Institute of Computer Integrated Manufacturing for Sustainable Innovation (ICIMSI), Centro Galleria 2, Manno, CH-6928, Switzerland, Department of Chemistry, Texas A&M University, College Station Texas 77843, and Department of Pharmaceutics and Biopharmacy, Philipps Universität, Marburg, Germany

Abstract

In this study, simulation challenges intuitive models of "flexible" and "rigid" generation two triazine dendrimers as it pertains to solution conformation and conformation on binding DNA or siRNA sequences. These results derive from structural and energetic analyses of the binding events. Simulations of the rigid structure reinforce the role of the constrained piperazine linker in positioning the peripheral groups at significant distance from each other and the core of the dendrimer. In contrast, the flexible dendrimer, characterized by triethyleneglycol-like linkers, collapses in solution. On binding DNA and siRNA, these conformations are largely retained. The rigid dendrimer undergoes reorganization of peripheral groups to generate a large number of contacts to the nucleic acid. In contrast, the flexible dendrimer, originally conceived to create multivalent interactions with nucleic acids, generates only a few contacts and collapses further. This paper provides unique insight in the role played by molecular flexibility in the binding phenomenon.

Introduction

Chemical intuition and simple back-of-the-envelope calculations provide useful molecular descriptors including adjectives like "flexible" and "rigid". Such terms are especially common when discussing the linking domains between divalent ligands. Lately, flexibility and rigidity parameters were listed as one of the five critical nanoscale design parameters (CNDPs; i.e., size, shape, surface chemistry, flexibility/rigidity, and architecture) that must be taken into account in the exploration of the behavior of well-defined nanoscale building blocks such as dendrimers.[1] Indeed, these terms create useful mental imagery for what may likely be occurring in binding ligand interactions with either multiple primary sites or primary and secondary sites on a complex biological target. It seems reasonable to assume that linker flexibility would enhance the binding avidity of ligands due to the ability to more readily adopt conformations that allow for interactions with the binding site. Indeed, this effect has been observed by Frey et al. who showed that multiple bonds between the ligand

[*]To whom correspondence should be addressed. giovanni.pavan@supsi.ch..
[†]SUPSI.
[‡]Texas A&M University.
[§]Philipps Universität.

Supporting Information Available. Complete radius of gyration plots for solution phase dendrimers and tables containing per-residue decomposition energies. This material is available free of charge via the Internet at http://pubs.acs.org.

and the target reduce the binding by 50% as compared to ligands attached by only a single bond.[2] However, other studies have described an alternative scenario. Krishnamurthy et al. have suggested that linker flexibility has negligible effect on the avidity of ligand binding.[3] This study was corroborated by Handl et al., wherein they observed only minor improvements to binding using more flexible linkers.[4] Vagner et al. have shown that binding avidity is enhanced using more rigid linkers as compared to the more flexible analogues.[5]

Intuition is further compromised when the constructs are multivalent and the number of atoms involved in ligand/target binding becomes large. As it pertains to dendrimers and other globular macromolecules, we have been content to consider these structures as hard spheres at suitable generation numbers.[6] In many cases, this assumption is unsuitable: the onset of interesting biological activities of these structures occurs at low generations before the hard-sphere model is relevant. Furthermore, the equilibrated conformations of dendrimers have been shown to be dramatically influenced by the flexibility of the linking groups of the monomer units. Flexible dendrimers have been shown to adopt a dense core structure due to backfolding,[7–9] while this is not observed for the rigid analogues.[10–12] Furthermore, the structure of dendrimers in solution has been shown to be independent of concentration, unlike the linear polymer analogues.[13] In this context, the descriptors “rigid” and “flexible” might adequately refer to local structure but do not necessarily communicate global structure for dendrimers.

Interest in the use of triazine dendrimers to deliver nucleic acids to cells led to the examination of a family of dendrimers that were described (perhaps naively) as “rigid”, “semi-rigid”, and “flexible”. Initially, we hypothesized that rigid dendrimers would engage in limited contacts with nucleic acid, positioning only a limited number of cationic groups near phosphates to engage in productive electrostatic interactions, as shown in Scheme 1. The framework of the “rigid” dendrimer would necessitate that other potential binding cationic amines with binding potential would be arrayed into solution. In contrast, the mental model for the “flexible” dendrimer comprised a fluid molecule that advantageously placed a large number of cationic amines in close proximity to the anionic phosphate backbone. The initial libraries of dendrimers were designed to include cationic amine groups linked by seven atoms, -CH_2CH_2-$CH_2NCH_2CH_2CH_2$-, a linker that was hypothesized to be both innocuous and would afford an opportunity to place two amines such that they could interact with a single phosphate group or perhaps neighboring phosphate groups.

The impact that composition had on the biological and physicochemical properties of these dendrimers was validated in a number of assays, including overall transfection efficiency, toxicity (determined using both MTT and hemolysis assays), zeta potential, complex size, and the ability to exclude ethidium bromide.[14,15] The molecular bases for differences in these characteristics was not entirely clear, which prompted the use of computation to provide a better foundation for intuition and to guide the design of triazine dendrimers in future transfection studies. Here, we examine two dendrimers using simulation. The nomenclature is preserved from our initial reports. The “rigid” dendrimer, **G2–5**, is a second generation molecule that displays 12 cationic amines and 6 hexyl chains. The second generation, “flexible” dendrimer, **F2–1**, displays 12 cationic amines and 12 hydroxyl groups. These molecules are shown in Scheme 2. We chose to start with these two dendrimers because they vary in a number of different properties, including core scaffolding and functionalization on the periphery.

A universal color scheme is adopted throughout the manuscript.**F2–1** was hypothesized to be flexible based on the ethyleneglycol chain (yellow). In contrast, **G2–5** was envisioned to be more rigid due to the limited conformations allowed by the piperazine ring (yellow). The bifurcated cationic peripheral group was envisioned to be capable of interacting with

multiple phosphate groups either within a single strand or by bridging a groove. Additionally, two different auxiliary binding groups, a hexyl group and a diol, are probed (red).

The multivalent recognition of DNA and siRNA by these macromolecules is strictly related to their structural flexibility. In fact, their multivalency is represented by the ability to orient and use their surface charges in a cooperative[16] way to bind nucleic acids with high affinity and reducing the entropic cost of the process.[17,18] To understand how molecular flexibility affects the interactions with nucleic acids, we created models of these triazine dendrimers in complex with DNA and siRNA in 1:1 ideal ratio. This was already considered a reliable model of binding in our previous work[19] and a suitable method to explore the details of binding.

In summary, we find that simulation challenges most of these preconceived intuitions of binding.

Materials and Methods

DNA and siRNA Sequences

DNA was modeled using a 21-base double strand in B-form. The length matches the siRNA sequence referred to as GL3. The dendrimers modeled are smaller than these sequences, and accordingly, these dimensions are a reasonable compromise of binding phenomenon in 1:1 ratios and computational investment. A similar strategy has been employed earlier to model dendritic spermine derivatives.[19] The sequences of siRNA are 5′-UCG AAG UAC UCA GCG UAA G dTdT-3′ and 3′-dTdT AGC UUC AUG AGU CGC AUU C-5′. The sequence of DNA strands are 5′-TCG AAG TAC TCA GCG TAA GTT-3′ and 3′-AGC TTC ATG AGT CGC ATT CAA-5′.

Dendrimers

The dendrimer structures synthesized were composed of different residues: a central core (CEN), the variable linker (LIN), a peripheral triazine (PER), auxiliary groups (END), and surface charged ligands (POS) each with a +1 charge, making the global dendrimer charge +12 at neutral pH. Parameters for these residues were calculated with ab initio techniques.

Molecular Dynamic Simulations

All simulations and data analyses were performed with the AMBER 10 suite of programs.[20] The force field parameters for these residues were obtained using the *antechamber* module of AMBER 10. The **G2–5** and **F2–1** dendrimers were solvated in a TIP3P water box,[21] extending 12 Å from the solute in three dimensions. A suitable number of counterions were added to neutralize the system using the *leap* module of AMBER 10, and overlapping water molecules were removed. The resulting systems, which contained the dendrimer, ions, and water, were first minimized and then equilibrated by running 10 ns NPT molecular dynamics simulations.

After the equilibrated dendrimers were obtained (Figure 2), the water molecules and counterions were removed and **G2**–**5** and **F2**–**1** molecules were then placed in close proximity to the major grooves of DNA and siRNA. Both complexes were again solvated with a water box extending 12 Å from the solute. The proper number of cations was added to reproduce system neutrality, followed by the inclusion of additional NaCl to achieve the correct experimental salt concentration in relation to the volumes of the corresponding water box. Overall, four molecular systems were prepared: **G2**–**5** or **F2**–**1** in complexation with

either DNA or GL3 siRNA at an ionic strength of 150 mM NaCl. Table 1 summarizes the main characteristics of the simulated systems.

All the molecular systems were minimized and then equilibrated at 300 K by 50 ps molecular dynamics under NVT conditions. This stage was followed by a density equilibration run (50 ps) under NPT conditions. The production dynamic lasted for 15 ns under periodic boundary condition at 300 K and 1 atm using a time step of 2 fs, the Langevin thermostat, and a 10 Å cutoff. To treat long-range electrostatic effects, the particle mesh Ewald[22] (PME) approach was adopted, and the SHAKE algorithm[23,24] was used to constrain all bonds involving hydrogen atoms.

All of the molecular dynamics (MD) simulations were carried out using the *sander* and *pmemd* module within the AMBER 10 suite of programs, and the *parm99* all-atom force field by Cornell et al.[25] working in parallel on 128 processors of the Rosa Cray XT5 calculation cluster of the CSCS Swiss National Supercomputer Centre of Manno (Switzerland).

Energetic and Structural Analyses

All energetic analyses for each molecular system were performed by taking 200 unbound dendrimer and DNA/siRNA snapshots from the equilibrated phase of a single 15 ns MD trajectory. The ligand/receptor binding free energy, ΔG_{bind}, was calculated using the molecular mechanics/Poisson–Boltzmann surface area method (MM-PBSA),[26] as shown in eq 1.

$$\Delta G_{\text{bind}} = \Delta H_{\text{bind}} - T\Delta S_{\text{bind}} \quad (1)$$

$$\Delta H_{\text{bind}} = \Delta E_{\text{int}} + \Delta G_{\text{sol}} \quad (2)$$

The enthalpic contribution was calculated by summing the in vacuo gas-phase energies ($\Delta E_{\text{gas}} = \Delta E_{\text{ele}} + \Delta E_{\text{vdw}}$) and the solvation free energies ($\Delta G_{\text{solv}} = \Delta G_{\text{PB}} + \Delta G_{\text{NP}}$).[27]

The Poisson–Boltzmann (PB) approach[28] was used to calculate the polar component of ΔG_{solv}, while the nonpolar contribution to the solvation energy was calculated as $\Delta G_{\text{NP}} = \gamma(\text{SASA}) + \beta$, in which $\gamma = 0.00542$ kcal/Å^2, $\beta = 0.92$ kcal/mol, and SASA is the solvent-accessible surface area estimated with the MSMS program.[29] To compute the entropic contributions ($-T\Delta S$), the normal-mode[30] analysis was applied to 100 MD frames.

As described in more detail in further sections, the individual contribution to the polynucleotide binding of each dendrimer residue was assessed by further processing the MD frames, using the *mm_pbsa.pl* script of AMBER 10 to decompose the total interaction energy on a per-residue base.

The *ptraj* module of AMBER 10 was used to process the dynamic trajectories to obtain relevant geometric data of all the complexes (i.e., root-mean-square deviations (rmsd), radii of gyration, and radial distribution functions (RDF)).

Results and Discussion

Solution Phase Structures of F2–1 and G2–5

As a starting point for the study, the solution phase structures of **F2–1** and **G2–5** were calculated in a cubic periodic water box containing a suitable number of Na^+ and Cl^- ions to guarantee neutrality and to achieve 150 mM salt concentration, an environment that mimics

physiological solution. Computation provided radius of gyration (R_g) profiles and radial distribution functions (RDF) that showed that the behaviors of **F2–1** and **G2–5** are notably different.

The radius of gyration R_g as defined by eq 3 is not a true measurement of the molecular radius. Instead, it is the average distance between each atom and the center of mass of the structure considered.

$$R_g{}^2 = \frac{1}{N}\sum_{k=1}^{N}(r_k - r_{mean})^2 \quad (3)$$

Based on a recent study, it has been observed that the length of the linker groups between monomer units of a dendrimer have little effect on the dendrimer conformation. In a good solvent, the linker groups effectively behave as unperturbed blobs that rearrange only to minimize excluded volume interactions.[31] However, these trends differ from the structural changes observed for the dendrimers investigated in this study. While the rigidity of **G2–5** is reflected in a flat R_g plot over the solution phase simulation, **F2–1** undergoes significant reorganization. This reorganization of the flexible dendrimer is captured in both the final structure and calculated radius of gyration, as shown in Figure 2 (the original R_g plots available in the Supporting Information). Here, the R_g value observed for **G2–5** is calculated to be 13.5 Å, almost identical to the value observed for the starting structure and consistent with a rigid framework. In contrast, **F2–1** reorganizes by collapsing from an initial, extended structure measuring 25 Å to a compact equilibrated globule of 10.7 Å, corresponding to a significant reduction in radius of gyration.

The final equilibrated solution energies calculated for **F2–1** and **G2–5** (−8.9 and −4.4 kcal mol^{-1}, respectively) reflect the differences in intrinsic rigidity of these two structures. The highly flexible linkers of **F2–1** collapse near the core, creating a barrier between the external solvent and the hydrophobic triazine unit. On the other hand, the intrinsic rigidity of **G2–5** precludes collapse: only minor adjustments of surface groups are observed. This inability of **G2–5** to reorganize explains why the energy of the equilibrated configuration of **F2–1** in salt solution is almost two times lower as that of **G2–5** in the same conditions.

The radial distribution functions (RDFs) plot the number of atoms belonging to both the dendrimer and the solvent molecules at specific distances from the center of mass of the dendrimer at each simulation step. The results are shown in Figure 3. The curves reported are average values for the RDFs along the last 2 ns of the equilibrated dynamic and, thus, represent the density of atoms in space with respect to time. It is worth noting that high peaks in a certain zone of these graphs correspond to areas of high atomic density and low atomic mobility. The trace for **G2–5** suggests “molecular porosity”. That is, the center of mass of the dendrimer shows an area of high atomic density at 2–3 nm from that falls off rapidly, as well as a clustering of peripheral groups represented as broad peaks appearing from 10–18 nm. This nonuniformity in peak height in the RDF profile suggests a difference in the ability of the two regions to readily vibrate. The rigid core region is forbidden from free vibrations in comparison to the oscillations that occur at the periphery of the dendrimer. In contrast, **F2–1** plots slope consistently, with a dense center-of-mass structure having high atomic density observed at small radii. Here, the RDF plots are very close to the one typical of PAMAM dendrimers reported by previous modeling studies.[32,33] Differences in structure are also revealed by accessibility of solvent molecules to the center of mass. **G2–5** reveals porosity with the sharp increase in water density observed at 3 nm. Solvent density is largely uniform throughout. In contrast, solvent is more excluded from **F2–1** by the PEG-like

linkers. This trend is shown by the gradual onset of solvation, presumably due to a largely inaccessible center of mass.

Interactions with DNA and siRNA

We rely on the data obtained from ethidium bromide exclusion assays to anchor our intuition on nucleic acid binding. Experimentally, the binding of **G2**–**5** and **F2**–**1** to DNA was estimated using an ethidium bromide (EthBr) exclusion assay. In this assay, 4 μg of herring testes DNA was complexes with increasing amounts of dendrimer and diluted to a final volume of 280 μL. Following a 20 min incubation period, the complexes were treated with 20 μL of 0.1 mg/mL ethidium bromide solution, and intercalation-induced fluorescence was quantified using a fluorescence plate reader. The results of this assay are reported as both a C_{50}, which represents the concentration of dendrimer require to exclude 50% of EthBr, and converted mathematically to a CE_{50}, which represents the N/P ratio required to exclude 50% of EthBr. The results are shown in Table 2.[14,15]

Ethidium bromide intercalation occurs when the DNA is not “protected” by dendrimer. Increased ethidium bromide intercalation at a given DNA concentration corresponds to lesser DNA binding by the dendrimer. Accordingly, lower C_{50} and CE_{50} values reflect more effective DNA binding. Defining “more effective” unambiguously is difficult: in these studies, “more effective” could be reflected either in binding constant or size of the footprint of the dendrimer on the DNA.

For the purpose of modeling, equilibrated solution phase structures of free **G2**–**5** and **F2**–**1** were taken as a starting point for the creation of all the complexes. Dendrimer–nucleic acid complexes were assembled by placing the dendrimer in close proximity to the major groove of the nucleic acid of interest and immersing the structure in the periodic water cube in presence of salt ions to reproduce neutrality and a 150 mM salt concentration.

As expected, the interaction between the dendrimer and the nucleic acid structure result in no significant changes in the conformation of the oligonucleotide. This result follows trends observed in previous reports, which illustrate that the adsorption energy between a small cationic nanoparticle ($R \sim 15$ Å) and a polyelectrolyte are not large enough to overcome the bending rigidity of the electrolyte.[34] However, while the minimized structures of dendrimer and nucleic acid preserve the gross equilibrated confirmations of both the starting materials, more subtle differences emerge. Figure 4 shows the different behaviors of **G2**–**5** and **F2**–**1** upon binding to DNA and siRNA. The rigidity of **G2**–**5** places the cationic peripheral groups at a greater distance from the center of mass, promoting interactions with a larger area of the nucleic acid. This “footprint” is reflected in data collected from ethidium bromide titrations (Table 2). “Rigidity” is manifest in this structure: it can be thought of as a rigid molecular chassis with charged terminal units attached to the surface that reorient slightly to interact with the nucleic acid target. Similar reorganization occurs with the peripheral groups of **F2**–**1**, but the initial hypothesis that the flexible tethers would provide a more fluid and expanded binding domain is not borne out in these computations (Figure 1). Instead, **F2**–**1** largely maintains a tight, globular domain when exposed to polynucleotides, in analogy, for instance, to the classical PAMAM dendrimers.

Modeling the Binding Affinity of Dendrimers toward Nucleic Acids

To better understand these models, we performed energetic and structural analyses of the complexes. Moreover, we analyzed **G2–5** and **F2–1** dendrimers also for binding to siRNA to understand the effect of a different nucleic acid on the behavior of these molecules. Table 3 summarizes the free energies of binding of the dendrimers with the nucleic acids of interest (either DNA or siRNA). In all cases, association is promoted by favorable enthalpic

interactions at an entropic penalty. Presently, there appears to be no relationship between either dendrimer composition or nucleic acid and the magnitude of the gain or penalty. Perhaps surprisingly, the relative rigidity of **G2–5** does not communicate fewer entropic penalties in light of fewer enthalpic interactions, nor does the flexible **F2–1** show enhanced enthalpic gain at the cost of entropic penalty. Table 3 reports the energetic values normalized over the number of primary binding groups (i.e., the 12 cationic amines of each dendrimer) to afford direct comparisons with other systems and to explore the ability of each structure to use effectively its active groups. For calibration, spermine-decorated dendrons[35] considered "ultra high affinity binders"[19] showed similar albeit slightly higher normalized binding energy values of about −7 to −8 kcal mol^{-1}, while values for PAMAM dendrimers currently under investigation are slightly lower.

Binding reflects a compensation between enthalpy and entropy as might be expected. The entropic penalties assessed in orienting cationic surface groups toward the negatively charged phosphate atoms in either DNA or siRNA is rewarded with favorably binding interactions. The high affinity of each charged group of **G2–5** for siRNA corresponded to an enthalpic gain of −12.8 kcal mol^{-1} and an entropic penalty of +5.7 kcal mol^{-1}. Conversely, the low affinity of each charged group of **F2–1** for DNA is due to a low enthalpic gain of −8.4 kcal mol^{-1} at the consistent entropic cost of +4.7 kcal/mol.

Table 3 shows that, while **G2–5** reports high affinity, **F2–1** shows a consistently lower affinity for both ligands. The loss in affinity is given by the decrease in the favorable enthalpic term (ΔH_{bind}) of **G2–1** and **F2–1** of ~25% in DNA and ~40% in siRNA binding. However, due to the higher rigidity of DNA, the entropic cost required to **F2–1** for a successful binding with DNA is higher than for siRNA (+4.7 vs +3.5 kcal mol^{-1} respectively), and this produces a lower per-charge affinity (ΔG_{bind} is −3.7 and −4.5 kcal mol^{-1} if **F2–1** is binding DNA and siRNA, respectively). These data indicate that the enthalpic contribution to binding is strongly electrostatically driven in these binding phenomena, **F2–1** is not able to effectively use the potential of its charged amines.

Radii of Gyration

An additional layer of insight is offered by examining the radii of gyration of these complexes, which has been averaged over the last 2 ns of simulation. Table 4 reports the radii of gyrations (R_g) for complexes (dendrimers+oligonucleotides), DNA/siRNA molecule, dendrimers, and for the positive surface ligands (POS), as well as shows the difference between the R_g of POS residues and the dendrimer, which is expressed as a percent (%var).

These values provide some insight into the level of reorganization in these globular structures. The R_g values calculated for the polynucleotides in the presence and absence of dendrimer are largely unchanged, suggesting that within these simulations, the structure of the polynucleotide is not grossly affected. The radius of gyration, R_g, reports the average distance between each atom and the center of mass of the macromolecule, which is not necessarily the core as depicted in a 2-D representation. We refer to this value loosely as "size" for the purpose of discussion. Our intuition is impacted in two ways by this data. First, the changes in "size" of the macromolecules on binding can be assessed by comparing the R_g of the native, unbound macromolecule and the bound species. Second, the changes in "conformation" of the macromolecules upon binding can be assessed by comparing the R_g of the dendrimer and simply that of the cationic end groups: that is, a large difference between R_g of whole dendrimers and surface ligands (%var) means a high degree of orientation of external charged groups extended toward the external salt solution or toward distant anionic groups. Based on results from previous studies, in which PAMAM dendrimers were shown to expand noticeably to optimize electrostatic interactions with

DNA,[36] we expected that the R_g for **G2–5** and **F2–1** would increase to improve binding interactions and that there would be little difference between the R_g of the macromolecule and that of the cationic end groups, suggesting that there dendrimers were orienting the charged groups on the periphery toward the oligonucleotides.

The data suggests that rigid **G2–5** dendrimer does not undergo significant changes in radii (which we correlate to gross orientation) on binding to either DNA or siRNA based on the similarity in radii (13.5 Å for the unbound **G2–5** vs 13.1 Å and 14.1 Å for **G2–5** complexed with DNA and siRNA, respectively). Indeed, similar binding strategies might be hypothesized. However, while **F2–1** does not undergo significant conformation changes on binding DNA (10.7 Å unbound vs 10.4 Å bound), it does reorganize on binding siRNA (R_g 9.6, indicating 10% change). This difference is likely due to the higher flexibility of siRNA strands, which are able to partially adapt to the small **F2–1**. During binding **F2–1** is thus allowed to collapse further and to maintain about the same enthalpic affinity than versus DNA at a reducing the entropic penalty of ~33% (Table 3). On binding either DNA or siRNA, the variability between end group R_g and global R_g for **G2–5** is small (%var ~ 3–6). Conversely, the %var of **F2–1** (~18–21) reflects reorganization. Here, the flexibility of PEG-like core is used to obtain a better orientation.

Radial Distribution Functions

The radial distribution profiles calculated over equilibrium structures for the last 2 ns of simulation suggests how the structures may behave in space over time. Specifically, the analysis provides clues as to how the atomic density varies about the center of mass. As in these plots, sharp peaks correspond to a large number of atoms confined both spatially and temporally. Broad features correspond to less confined, rapidly reorganizing domains (although we hesitate to say “flexible” based on our usage of this term). The discussion is subdivided by macromolecule in the following sections.

Macromolecule G2–5—The four plots shown in Figure 5 describe **G2–5** interactions with DNA (A,C) and siRNA (B,D) for all atoms (A,B) and for select atoms (C,D). The profiles in the top row reveal that bound **G2–5** behaves similar to free **G2–5** in solution, which was shown previously by the blue curves in Figure 3. That is, the distribution function reveals the “porosity” signature described earlier, whereby a sharp peak represents a dense core and a broader feature between 10–20 Å reveals more rapidly reorganizing peripheral groups.

The second row of traces shows the distribution profiles for the cationic groups (blue) and phosphates of the nucleic acids (pink). With DNA, sharp features at 4 and 7 Å for N and P atoms, respectively, reveal that one interaction occurs near the center of mass. Conceptually, we consider this an anchoring interaction, characterized by low mobility, because it is present in the same zone across the entire simulation. The tailing of the pink trace is expected: the nucleic acid is longer than the macromolecule. With siRNA, the pattern and its translation is consistent, but no interactions are occurring near the center of mass as indicated by the lack of sharp peak at distances less than 10 Å. However, the curves superimpose to create “binding space” at distances 10–15 Å from the center of mass, indicating a uniform binding without preferential binding spots.

Macromolecule F2–1—The radial distribution functions of **F2–1** interacting with DNA and siRNA are shown in Figure 6. As before, the top traces reveal that the general morphology has not changed significantly from the unbound forms: the dendrimer, as shown in Figure 3 (blue curve) remains a dense core structure. The broadening visible upon siRNA binding reflects the hypothesized swelling of the molecule. The lack of good overlap

between cationic nitrogen atoms of the dendrimer and phosphorus atoms of nucleic acid is evident from the distances between the electrostatic groups. Unlike the favorable distance translation of 3–4 Å observed for **G2–5**, the greater distances between binding groups suggests that interaction is more transient and involves more dynamic processes. Both the graphs related to **F2–1** binding DNA and siRNA show poor superposition between blue and pink profiles, indicating a different dynamic behavior of N and P atoms. Interestingly, Figure 6c shows a zone, between 15 and 22 Å, with nearly perfect N and P curve superposition. This low density zone is actually a high mobility binding zone, characterized by few binding spots composed by single N atoms of the dendrimer and P atoms of DNA that are strongly vibrating in the same way. The entire (albeit low) binding affinity between **F2–1** and DNA arises from this domain. However, the superposition in any zone of these RDF graphs is very low, indicating that the binding is punctuated and discontinuous.

Energetic Insight in the Binding

The simulations provide an opportunity to dissect additional detail on the molecular bases for binding. For this analysis, the dendrimers were divided into core domains (CEN, LIN, and PER residues) and surface cationic and auxiliary, neutral groups (POS and AUX, respectively). In the case of **G2–5**, the neutral AUX group was a single hexyl chain. For **F2–1**, the AUX groups are alcohols. The total interaction energies between dendrimers and oligonucleotides were divided to describe the interaction energy by residual base. This strategy allows for the calculation of the contribution that each residue gives to the binding affinity. The energetic components reported in Table 5 describe the differences between the energy of the dendrimer/DNA complex (E_{complex}) and the sum of the energies of dendrimer and DNA taken separately ($E_{\text{dendrimer}} + E_{\text{DNA}}$). A negative E value indicates the tendency of the dendrimer and DNA (or siRNA) have to form a complex according to eq 4.

$$E = E_{\text{complex}} - (E_{\text{dendrimer}} + E_{\text{DNA}}) \quad (4)$$

Gas-phase nonbond interaction energies (E_{gas}) for each residue are composed of electrostatic and van der Waals in vacuo contributions (E_{ele} and E_{vdw}, respectively) according to eq 5.

$$E_{\text{gas}} = E_{\text{ele}} + E_{\text{vdw}} \quad (5)$$

The in vacuo gas-phase energy for each residue (E_{gas}) is then corrected for solvation effects to give the total energy, E_{tot}, using the generalized Born[37] method that is available in the *mm_pb-sa.pl* script of AMBER 10, as the Poisson–Boltzmann method is not practical for decomposition calculations.

As predicted by intuition, the cores (CEN, LIN, and PER residues) of the dendrimers make no significant energetic contributions to binding (the Supporting Information tabulates contributions for all residues). Similarly, no benefit is derived, indeed only penalty, from other hydrophobic portions (AUX) of these molecules including the hexyl tails of **G2–5** ($E_{\text{tot}} \sim 0$ kcal mol^{-1}). Any peripheral group that links triazine to either cationic nitrogen or hydroxyl (i.e., the -N($CH_2CH_2CH_2X$)$_2$ groups of the peripheral triazine) typically costs 0–3.5 kcal/mol for each group. Thus, binding derives solely from interactions between the phosphate backbone and terminal POS groups. The potential binding affinity between the hydroxyls and DNA is largely negated by the costs of the linker displaying them. Table 5 summarizes the energetic contributions of the surface POS groups.

These calculations show that cationic groups can be categorized either as engaged or disengaged from interactions with the polynucleotide. Energies for engaged groups are

considerably high. Disengaged groups contribute nothing energetically as both distance and ions in solution effectively screen these interactions. For example, disengaged groups POS 5–POS 6 and POS 7–POS 8 of **G2**–**5** have no binding efficiency toward DNA. Instead, they act as an umbrella (Figure 7A), shielding the more crucial, binding residues from ion interference: this behavior has been observed in other structures.[19]

We can count the number of productive enthalpic interactions ($E_{tot} \leq -5.0$ kcal mol^{-1}) between dendrimer and target nucleic acid. **G2**–**5** makes seven cationic contacts (POS 1, 2, 3, 9, 10, 11, and 12) with DNA, while **F2**–**1** makes only four contacts (POS 1, 3, 7, and 10). Interestingly, when a peripheral group of **G2**–**5** makes contact with DNA, both cationic amines are engaged. In contrast, only one of the two available cationic groups of peripheral groups in **F2**–**1** make contact with DNA, albeit more strongly. This difference in binding geometry appears to be due to the interactions between the hydroxyls of the AUX (partial negative charge) and POS terminal groups of **F2**–**1**, wherein both hydroxyls capture one cationic group: the AUX groups of **G2**–**5** are hexyl chains. Fewer contacts with siRNA are recorded for both dendrimers: **G2**–**5** makes five contacts (POS 1, 2, 5, 6, and 8), which typically involve both cations of a peripheral group, while **F2**–**1** makes three contacts (POS 7, 8, and 10). In average, **F2**–**1** is less able to use productively its charged POS groups, as evidenced by the average E_{tot} value (−4.5 kcal mol^{-1} for **G2**–**5** vs ~–3.0 kcal mol^{-1} for **F2**–**1**, a 50% of difference). All of these interactions are captured in Figure 7.

It is worth noting that, for **F2**–**1**+siRNA complex, significant binding energy derives from the POS 7–POS 8 branch. However, the phosphate group does not sit symmetrically in the binding site and produces a nonuniformity in the siRNA and dendrimer vibrations. The red oval in Figure 7D identifies a hydrophobic patch of **F2**–**1** that remains exposed to siRNA. This zone of hydrophobic interaction correlates with the high pink peak in the RDF of Figure 6D at the distance of about 7 Å. Binding is not uniform, but characterized by a single point that acts as a “hinge” between **F2**–**1** and siRNA. Moreover, because the vibrations of dendrimer and nucleic acids are different, this peak relates to low mobility P atoms that create vibration conflicts with **F2**–**1** branches during the complex oscillation. Due to its compact conformation in solution, **F2**–**1** forms with nucleic acids a binding that is completely different from the one of **G2**–**5**. In fact, **F2**–**1** binds with DNA and siRNA as an external body, and thus, the product of binding is a compound of two molecules attached by single points. This makes binding less topologically uniform and dynamically stable. On the other hand, **G2**–**5** maintains a high uniformity in binding due to its open conformation. In this way, by distributing uniformly the binding between multiple contact points, **G2**–**5** is able to use its active sites with extremely high effectiveness, vibrating uniformly in complex with both DNA and siRNA.

Conclusions

In this modeling, differences in peripheral groups and core flexibility lead to quantifiable differences in the energetic of binding as well as different conformational responses within the macromolecule. These models offer a starting point for rationalizing the difference that is observed experimentally when **G2**–**5** and **F2**–**1** are used to bind to DNA or siRNA.

The **F2**–**1** structure was expected to engage polynucleotides of DNA and siRNA by extending its long and flexible PEG-like branches to maximize the number of productive interactions between cationic groups pendant and the anionic target. Indeed, the converse is true: the flexible linkers facilitate collapse of the structure protecting it from the external salt solution resulting in a reduction in the radius of gyration. The molecule assumes a spherical shape with a compacted core and strong orientation of the surface groups toward the ions in solution, the typical configuration assumed by PAMAM dendrimers. During binding with

oligonucleotides, this conformation does not change much, and **F2**–**1** binding focuses on single binding points characterized by high binding strength. This inability to compensate for the low number of interactions resulted from the binding site conformation and a nonuniformity in molecular vibration resulted in less stable binding. On the other hand, **G2**–**5** maintains a conformation that is more optimized to bind to oligonucleotides despite having a molecular conformation originally less stable in solution, the rigid hydrophobic core remained exposed to water and ions. Energetically, it appears that **G2**–**5** binds DNA and siRNA equally well, making, on average, more contacts with the polynucleotide than **F2**–**1**. In contrast, **F2**–**1** binds less efficiently. The structure of **F2**–**1**, originally designed to gain flexibility, resulted in a more compacted and rigid sphere-like conformation while in solution that minimized contacts with the nucleic acid. Interestingly, the binding with siRNA is favored over DNA due to the higher rigidity of DNA and to the consistent curvature of siRNA, the GL3 molecule can partially adjust on **F2**–**1**, reducing the entropic cost and thus enhancing binding (gain in ΔG_{bind} of >20%).

In this study, modeling is shown to be an ideal instrument to support the intuitive conception and the design of new binding agents. We believe that the results reported in this paper will give a new point of view in the binding mechanism with nucleic acids, highlighting the direct relationship that exist between structure and functionality of these binding agents.

Supplementary Material

Refer to Web version on PubMed Central for supplementary material.

Acknowledgments

G.M.P. and A.D. acknowledge the CSCS Swiss National Supercomputer Centre of Manno (Switzerland) for the support and for the generous access to the 22128 processors of the Rosa Cray XT5 supercomputer. E.E.S. thanks the N.I.H. (R01 GM 65460).

References and Notes

(1). (a) Tomalia DA. Soft Matter. 2010 DOI: 10.1039/b917370f. (b) Tomalia DA. J. Nanopart. Res. 2009; 11:1251–1310. [PubMed: 21170133]

(2). Olivier V, Meisen I, Meckelein B, Hirst TR, Peter-Katalinic J, Schmidt MA, Frey A. Bioconjugate Chem. 2003; 14(6):1203–1208.

(3). Krisnamurthy VM, Semetey V, Bracher PJ, Shen N, White-sides GM. J. Am. Chem. Soc. 2007; 129(5):1312–1320. [PubMed: 17263415]

(4). Handl HL, Sankaranaryanan R, Josan JS, Vagner J, Mash EA, Gillies RJ, Hruby VJ. Bioconjugate Chem. 2007; 18(4):1101–1109.

(5). Vagner J, Handl HL, Gillies RJ, Hruby V. J. Bioorg. Med. Chem. Lett. 2004; 14:211–215.

(6). Tomalia DA. Prog. Polym. Sci. 2005; 30:294–324.

(7). Rosenfeldt S, Dingenouts N, Ballauff M, Werner N, Vogtle F, Lindner P. Macromolecules. 2002; 35(21):8098–8105.

(8). Rosenfeldt S, Dingenouts N, Ballauff M, Lindner P, Likos CN, Werner N, Vogtle F. Macromol. Chem. Phys. 2002; 203(13):1995–2004.

(9). Dingenouts N, Rosenfeldts S, Werner N, Voegtle F, Lindner P, Roulamo A, Rissanen K, Ballauff M. J. Appl. Crystallogr. 2003; 36(3):674–678.

(10). Rosenfeldt S, Karpuk E, Lehmann M, Meier H, Lindner P, Harnau L, Ballauff M. ChemPhysChem. 2006; 7(10):2097–2104. [PubMed: 16977668]

(11). Rosenfeldt S, Dingenouts N, Poetschke D, Ballauff M, Berresheim AJ, Muellen K, Lindner P, Saalwaechter K. J. Lumin. 2005; 111(4):225–238.

(12). Rosenfeldt S, Dingenouts N, Potschke D, Ballauff M, Berresheim AJ, Muellen K, Lindner P. Angew. Chem., Int. Ed. 2004; 43(1):109–112.

(13). Rosenfeldt S, Ballauff M, Lindner P, Harnau L. J. Chem. Phys. 2009; 130:1–7.

(14). Mintzer MA, Merkel OM, Kissel T, Simanek EE. New J. Chem. 2009; 33:1918–1925.

(15). Merkel OM, Mintzer MA, Sitterberg J, Bakowsky U, Simanek EE, Kissel T. Bioconjugate Chem. 2009; 20(9):1799–1806.

(16). (a) Wong SY, Pelet JM, Putnam D. Prog. Polym. Sci. 2007; 32:799–837.(b) Tiera MJ, Winnik FM, Fernandes JC. Curr. Gene Ther. 2006; 6:59–71. [PubMed: 16475946]

(17). (a) Huskens J, Mulder A, Auletta T, Nijhuis CA, Ludden MJW, Reinhoudt DN. J. Am. Chem. Soc. 2004; 126:6784–6797. [PubMed: 15161307] (b) Doyle EL, Hunter CA, Philips HC, Webb SJ, Williams NH. J. Am. Chem. Soc. 2003; 125:4593–4599. [PubMed: 12683831]

(18). (a) Lim CW, Ravoo BJ, Reinhoudt DN. Chem. Commun. 2005:5627–5629.(b) Mart RJ, Liem KP, Wang X, Webb SJ. J. Am. Chem. Soc. 2006; 128:14462–14463. [PubMed: 17090021]

(19). Pavan GM, Danani A, Pricl S, Smith DK. J. Am. Chem. Soc. 2009; 131(28):9686–9694. [PubMed: 19555062]

(20). Case, DA.; Darden, TA.; Cheatham, TE., III; Simmerling, CL.; Wang, J.; Duke, RE.; Luo, R.; Merz, KM.; Pearlman, DA.; Crowley, M.; Walker, RC.; Zhang, W.; Wang, B.; Hayik, S.; Roitberg, A.; Seabra, G.; Wong, KF.; Paesani, F.; Wu, X.; Brozell, S.; Tsui, V.; Gohlke, H.; Yang, L.; Tan, C.; Mongan, J.; Hornak, V.; Cui, G.; Beroza, P.; Mathews, DH.; Schafmeister, C.; Ross, WS.; Kollman, PA. AMBER. Vol. 10. University of California; San Francisco: 2008.

(21). Jorgensen WL, Chandrasekhar J, Madura JD, Impey RW, Klein ML. J. Chem. Phys. 1983; 79:926–935.

(22). Darden T, York D, Pedersen L. J. Chem. Phys. 1998; 98:10089–10092.

(23). Ryckaert J-P, Ciccotti G, Berendsen HJ. J. Comput. Phys. 1977; 23(3):327–341.

(24). Krautler V, Van Gunsteren WF, Hunenberger PH. J. Comput. Chem. 2001; 22(5):501–508.

(25). Cornell WD, Cieplak P, Bayly CI, Gould IR, Merz KM Jr, Ferguson DM, Spellmeyer DC, Fox T, Caldwell JW, Kollman PA. J. Am. Chem. Soc. 1995; 117(19):5179–5197.

(26). Srinivasan J, Cheatham TE III, Cieplak P, Kollman PA, Case DA. J. Am. Chem. Soc. 1998; 120(37):9401–9409.

(27). Jayaram B, Sprous D, Beveridge DL. J. Phys. Chem. B. 1998; 102(47):9571–9576.

(28). Sitkoff D, Sharp KA, Honig B. J. Phys. Chem. 1994; 98(7):1978–1988.

(29). Sanner MF, Olson AJ, Spehner J-C. Biopolymers. 1996; 38(3):305–320. [PubMed: 8906967]

(30). Andricioaei I, Karplus M. J. Chem. Phys. 2001; 115(14):6289–6292.

(31). Klos JS, Sommer J-U. Macromolecules. 2009; 42(13):4878–4886.

(32). (a) Maiti PK, Cagin T, Wang GF, Goddard WA. Macromolecules. 2004; 37:6236–6254.(b) Maiti PK, Cagin T, Lin ST, Goddard WA III. Macromolecules. 2005; 38:979–991.

(33). Han M, Chen P, Yang X. Polymer. 2005; 46:3481–3488.

(34). Ulrich S, Laguecir A, Stoll S. Macromolecules. 2005; 38(21):8939–8949.

(35). Konstiainen MA, Hardy JG, Smith DK. Angew. Chem., Int. Ed. 2005; 44(17):2556–2559.

(36). Maiti PK, Bagchi B. Nano Lett. 2006; 6(11):2478–2485. [PubMed: 17090077]

(37). Kollman PA, Massova I, Reyes C, Kuhn B, Huo S, Chong L, Lee M, Lee T, Duan Y, Wang W, Donini O, Ciplak P, Srinivasan J, Case DA, Cheatham TE III. Acc. Chem. Res. 2000; 33(12): 889–897. [PubMed: 11123888]

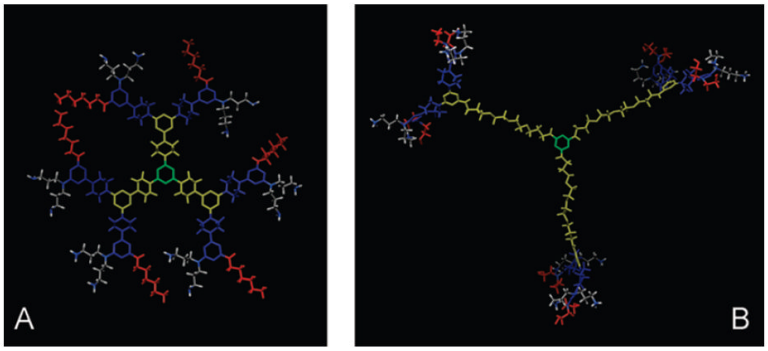

Figure 1.
Initial structural conformations of **G2–5** (A) and **F2–1** (B) molecules. The central core, CEN, residue is colored in green, the variable linkers, LIN, in yellow, peripheral triazines, PER, in blue, auxiliary, AUX, in red, and positive groups, POS, in native color.

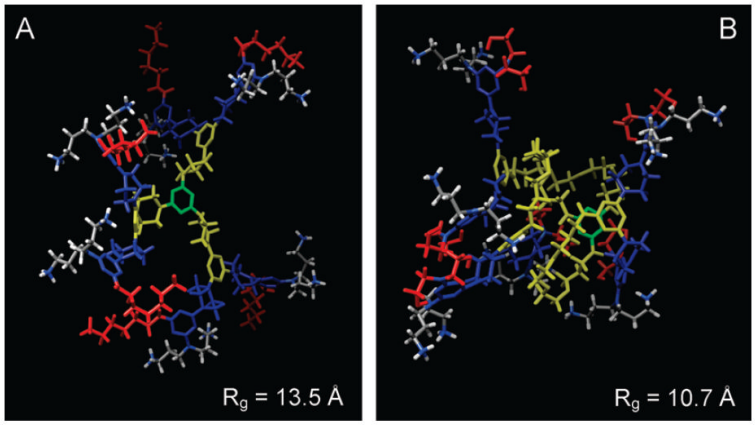

Figure 2.

Equilibrated structures of **G2–5** (A) and **F2–1** (B) and corresponding R_g values, expressed in Angstroms (Å). The dendrimer residues are represented using the same color scheme as in Figure 1. Water molecules and couterions have been omitted for clarity.

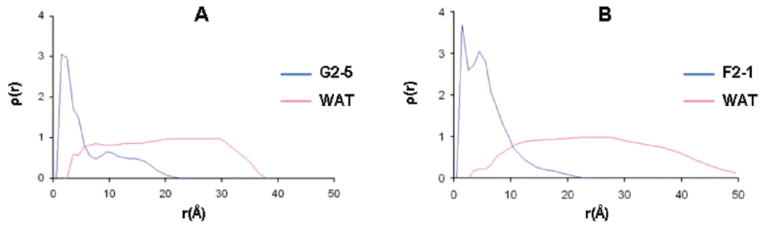

Figure 3.
Radial distribution profiles (RDF) of **G2–5** (A) and **F2–1** (B). RDF are reported for dendrimer (**G2–5** and **F2–1**: blue) and water (WAT: pink). Distances from the center of mass of the dendrimers are expressed in Angstroms.

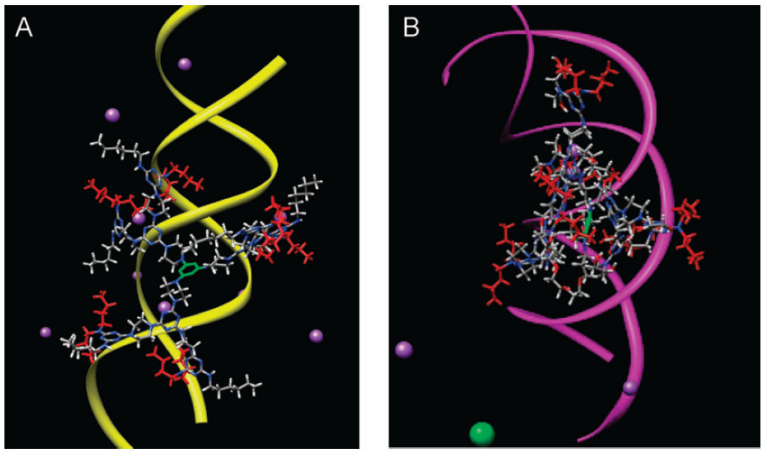

Figure 4.

Front view snapshots taken from the dynamic simulations of **G2**–**5**+siRNA (A) and**F2**–**1**+DNA (B). Dendrimers are colored by atoms except for CEN residues, colored in green, and POS surface groups, colored in red. Na^+ and Cl^- ions are purple and green spheres, respectively. GL3 siRNA and DNA are represented respectively as yellow and purple solid ribbon. Water molecules are omitted for clarity and only those counterions in close proximity to the complexes are shown.

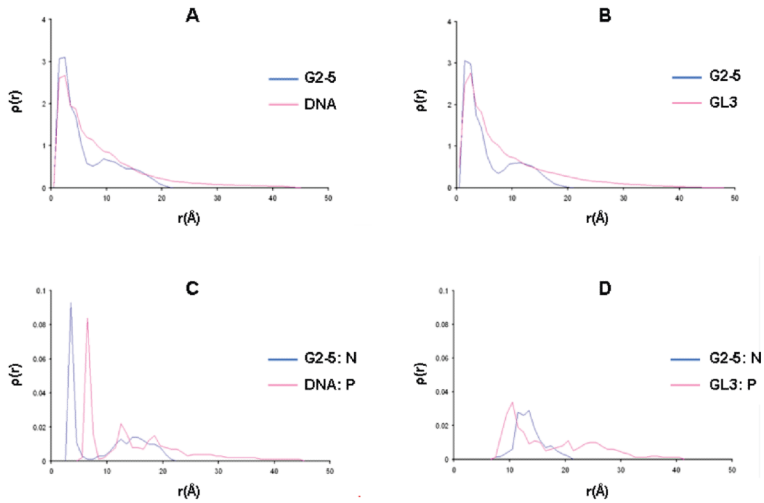

Figure 5.

Radial distribution functions of **G2–5** with DNA (A,C) and siRNA (B,D). The top traces (A,B) show the profile for all atoms of dendrimer (blue) and nucleic acid (pink). The bottom traces (C,D) show peripheral cations (blue) of the dendrimer and phosphorus atoms (pink) of the nucleic acid. Distances from dendrimer center of mass are expressed in Angstroms.

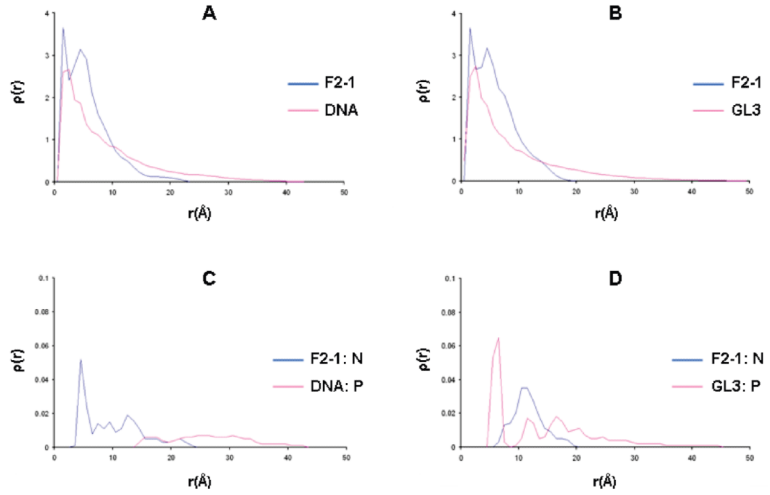

Figure 6.

Radial distribution functions of **F2**–**1** with DNA (A,C) and siRNA (B,D). The top traces (A,B) show the profile for all atoms of dendrimer (blue) and nucleic acid (pink). The bottom traces (C,D) show peripheral cations (blue) of the dendrimer and phosphorus atoms (pink) of the nucleic acid. Distances from the dendrimer center of mass are expressed in Angstroms.

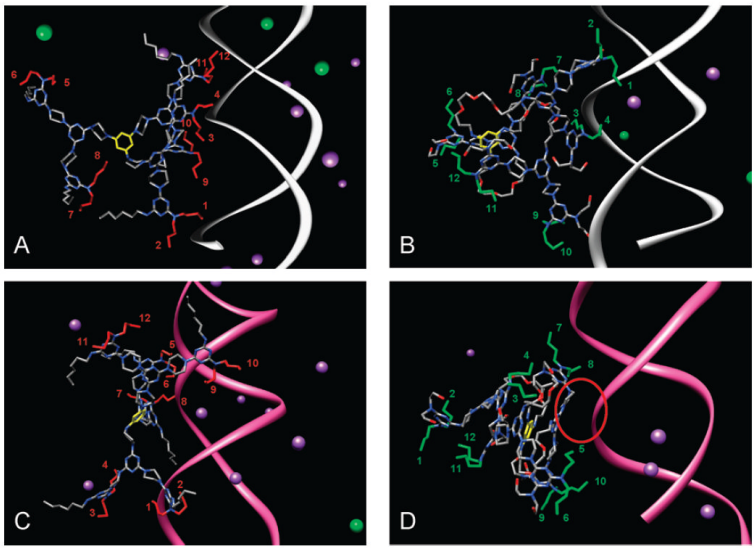

Figure 7.

Snapshots of dynamics simulation of (A) **G2**–**5**+DNA, (B) **F2**–**1**+DNA, (C) **G2**–**5**+siRNA, and (D) **F2**–**1**+siRNA. Within the dendrimer CEN is shown in yellow, LIN, PER, and AUX are colored using typical atom conventions, and the surface charged POS in red and green for **G2**–**5** and **F2**–**1**, respectively. Each POS residue is identified by a numerical index. Water molecules and hydrogens are omitted for clarity, and only those counterions in close proximity to the complexes are shown. DNA and siRNA are represented as solid ribbons colored in gray and pink, respectively.

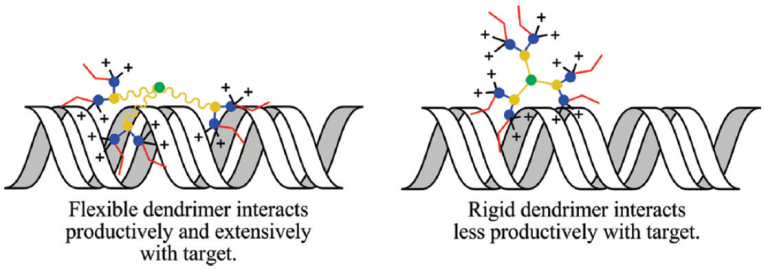

[a] The color scheme is preserved throughout.

Scheme 1.
Theoretical Binding Model for Flexible and Rigid Dendrimers with DNA[a]

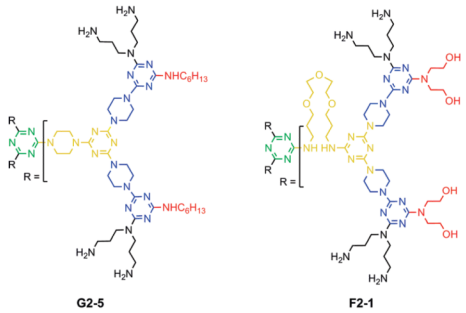

[a] The color scheme is preserved throughout the computational models with the core shown in green, the variable domain (rigid or flexible linker) in yellow, the peripheral triazine in blue, the cationic groups in native color, and the auxiliary binding group (either hydroxyl or alkyl chains) in red.

Scheme 2.

Dendrimers Used in this Study Include the “Rigid” **G2–5** and “Flexible” **F2–1**[a]

Table 1

Main Features of the Molecular Systems Simulated in this Work

complex	dendrimer charge	polynucleotide charge[a]	water box volume (Å)[18]	number of Na^+ and Cl^- atoms[b]	number of water molecules	total number of atoms in the system
G2–5+DNA	+12	−40	341024	62	10726	34052
G2–5+siRNA	+12	−40	324649	60	10189	32439
F2–1+DNA	+12	−40	304587	54	9371	30324
F2–1+siRNA	+12	−40	290165	52	9048	29053

[a] Both 21 base-pair DNA and siRNA have an overall charge of −40 because the terminal nucleotides do not carry a charge in the model.

[b] The total amount of counterions is the sum of the Na^+ and Cl^- atoms required for system neutralization of the systems and reproduce the 150 mM ionic concentration.

Table 2

Experimental Data for the Binding of **G2–5** and **F2–1** to DNA, as Determined by EthBr Displacement Assay[a]

dendrimer	C_{50}[b] (nM) 150 mM NaCl	CE_{50}[c] 150 mM NaCl
G2–5	2	0.5
F2–1	11	2.9

[a] Higher C_{50} and CE_{50} values represent less effective binding of the dendrimer to DNA.

[b] C_{50} represents the concentration (in nM) of dendrimer required to displace 50% of the EthBr ([DNA Base] = 1 μM, [EthBr] = 1.26 μM).

[c] CE_{50} represents the charge excess (ratio of protonatable nitrogen atoms on the dendrimer to deprotonatable phosphate groups on the DNA) at which 50% of EthBr is displaced.

Table 3

Free Energies of Binding Normalized per Charged Amine, Expressed as the Sum of the Enthalpic and Entropic Contributions[a]

dendrimers	ΔH_{bind}	$-T\Delta S_{bind}$	ΔG_{bind}
G2–5+DNA	−10.6 ± 0.7	+3.9 ± 1.0	−6.7
G2–5+GL3	−12.8 ± 1.0	+5.7 ± 1.6	−7.1
F2–1+DNA	−8.4 ± 0.6	+4.7 ± 0.7	−3.7
F2–1+GL3	−8.0 ± 0.6	+3.5 ± 0.6	−4.5

[a] Energies are expressed in kcal mol^{-1}.

Table 4

Radius of Gyration (R_g, Eq 3) of the Complex, as Composed by Dendrimer and Oligonucleotide, of the Single Nucleic Acid (DNA or siRNA), the Whole Dendrimer, the Surface Charged Groups (POS Residues), and the %var lndex[a]

systems	R_g complex (Å)	R_g, DNA and siRNA (Å)	R_g, dendrimer in complex (Å)	R_gENP (Å)	%var
G2–5+DNA	21.3	21.0	13.1	13.9	5.7
G2–5+siRNA	19.3	19.1	14.1	14.6	3.4
F2–1+DNA	21.0	20.9	10.4	12.7	18
F2–1+siRNA	20.0	19.5	9.6	12.1	21

[a]All R_g are measured in Ä. The native dendrimers show radii of gyration of 13.5 and 10.7 Ä, respectively, for **G2–5** and **F2–1**.

Table 5

Energetic Contributions of POS Groups to Binding[a]

		G2–5+DNA		F2–1+DNA		G2–5+siRNA		F2–1+siRNA	
residue[b]	**No.**	E_{tot}[c]	**avg**[d]	E_{tot}[c]	**avg**[d]	E_{tot}[c]	**avg**[d]	E_{tot}[c]	**avg**[d]
POS	1	−9.9	−4.5	−5.1	−3.0	−6.3	−4.5	−0.1	−3.1
POS	2	−5.0		−0.2		−6.8		−0.2	
POS	3	−7.8		−14.7		−0.5		−0.3	
POS	4	−4.4		−0.1		−0.5		−0.4	
POS	5	−0.3		−0.2		−8.8		−4.0	
POS	6	−0.2		−0.1		−16.8		−0.9	
POS	7	−0.2		−7.1		−1.3		−9.8	
POS	8	−0.2		−0.4		−6.9		−11.1	
POS	9	−5.6		−0.1		−3.3		−0.9	
POS	10	−7.2		−8.2		−2.2		−9.2	
POS	11	−5.7		−0.2		−0.3		−0.4	
POS	12	−7.0		−0.3		−0.3		−0.3	
total POS		53.5		36.3		53.8		37.6	

[a] For each complex, the energetic contribution (E_{tot}) of all POS residues, the mean values calculated on all POS groups, and the total POS energetic value are reported. Each POS ligand is identified by residue numbers (No.). POS residues that belong to the same branch are coupled in the table. All energies are expressed in kcal mol^{-1}.

[b] Energetic values are reported for the most interacting (POS) residues only.

[c] E_{tot} represents the per residue total energy after correction for solvation.

[d] The mean E_{tot} value (avg) is calculated over all the POS active groups.